Band structure, intercalation, and interlayer interactions of transition-metal dichalcogenides: TiS_2 and $LiTiS_2$

Cyrus Umrigar,* D. E. Ellis, Ding-sheng Wang,† H. Krakauer,‡ and M. Posternak§
Department of Physics and Astronomy and Materials Research Center, Northwestern University, Evanston, Illinois 60201

(Received 7 December 1981; revised manuscript received 22 July 1982)

The layered structure dichalcogenide TiS_2 was studied in thin-film and bulk models, with the use of the self-consistent linearized augmented-plane-wave (LAPW) scheme. Band-structure calculations were performed on the single sandwich (S-Ti-S), the double sandwich $(S\text{-}Ti\text{-}S)_2$, and the bulk to reveal the strength and effect of interlayer interactions on the electronic structure. Comparisons are made with existing bulk band models. The fully intercalated $LiTiS_2$ compound was studied by the same LAPW methods. Changes in the electronic density of states and charge density induced by the alkali intercalate are described.

I. INTRODUCTION

There has been considerable interest in the structural, electrical, optical, and superconducting properties of the transition-metal dichalcogenides.[1] One of the distinctive properties of these materials is that most of them have a layered crystal structure consisting of chalcogen-metal-chalcogen sandwiches that are internally strongly bonded but are only weakly coupled to each other. Some of their physical properties, such as electrical conductivity and shear resistance, are highly anisotropic.[2] They can be cleaved easily into thin platelets. Several of these materials exhibit charge-density-wave phase transitions.[3] An interesting feature of these materials, which is related to the weak intersandwich interaction, is that they can be intercalated, i.e., foreign atoms can be introduced into the intersandwich region. This is a phenomenon of technological importance because of the possibility of the use of the alkali intercalated materials in lightweight batteries.[4] It has been found that in some of these materials a magnetic moment is developed upon intercalation with a transition metal.[5] Also, intercalation can either enhance or suppress the superconducting transition temperature.[6]

The fundamental nature of electronic states in TiS_2 and related materials has long been the subject of controversy from both experimental and theoretical points of view. The bulk band structure of TiS_2 has been calculated by several authors,[7–11] and the experimental literature has become very extensive. Nevertheless, it is still questionable whether "ideal" TiS_2 is a semimetal or semiconductor. With the advent of accurate band-structure methods for treating thin-film geometries it has become literally possible to take apart crystals in order to analyze interactions between atomic planes. In this way it becomes possible to make quantitative conclusions about critical features of the band structure, which have been previously discussed qualitatively on the basis of symmetry arguments. Since intercalation modifies the interlayer interactions it is important to develop consistent theoretical models for treating ideal host and intercalated systems. Such models will hopefully provide a basis for a better understanding of transport and excitation phenomena.

In this paper we study the intersandwich interaction of TiS_2 by calculating the band structure and density of states (DOS) of a single sandwich of TiS_2, a double sandwich $(S\text{-}Ti\text{-}S)_2$, and the bulk material, and comparing them with each other. The semirelativistic linearized augmented-plane-wave (LAPW) method is used for both thin-film and bulk calculations in order to make meaningful compar-

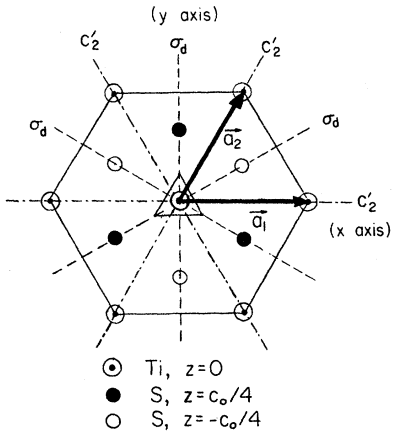

FIG. 1. Crystal structure of TiS_2.

TABLE I. Crystal structure constants and LAPW band parameters. All lengths in Bohr units. a_0 is the lattice constant in x-y plane, c_0 is the lattice constant in the z direction, u is the intrasandwich TiS_2 layer spacing, D is the boundary of film, D' is the distance used in defining the z-component Fourier expansion of LAPW's, and $\vec{k}$ points are wave vectors used in self-consistency iterations in units of $2\pi/a_0$, $2\sqrt{3}\pi/a_0$, $2\pi/c_0$.

	a_0	c_0	u	Muffin-tin radius Ti	Muffin-tin radius S	Muffin-tin radius Li	D	D'	$\vec{k}$ points used in self-consistent iterations
TiS_2 single sandwich	6.448		$0.25c_0$	2.78	1.813		9.007	12.0	$(\frac{2}{9},0),(\frac{4}{9},0),(\frac{5}{9},\frac{1}{3})$
$(TiS_2)_2$ double sandwich	6.448		$0.25c_0$	2.78	1.813		19.769	23.0	$(\frac{2}{9},0),(\frac{4}{9},0),(\frac{5}{9},\frac{1}{3})$
TiS_2 bulk	6.448	10.762	$0.25c_0$	2.78	1.813				$(0,\frac{2}{9},\pm\frac{1}{4}),(0,\frac{4}{9},\pm\frac{1}{4}),(0,\frac{8}{9},\pm\frac{1}{4})$ $(\frac{1}{9},\frac{5}{9},\pm\frac{1}{4}),(\frac{1}{9},\frac{7}{9},\pm\frac{1}{4}),(\frac{2}{9},\frac{8}{9},\pm\frac{1}{4})$
Li-$(TiS_2)_2$ sandwich	6.529		$0.232c_0$	2.78	1.813	2.5	20.765	23.0	same as TiS_2 sandwich
Li-TiS_2 bulk	6.529	11.707	$0.232c_0$	2.78	1.813	2.5			same as TiS_2 bulk

isons between different systems. The self-consistent band structures of both film and bulk predict that TiS_2 is a *semimetal,* in contrast to most previous work. We analyze the self-consistent valence charge density and decompositions of the density of states to obtain a bonding model consistent with the quasi-two-dimensional nature of the electronic structure. We have also studied the change in the electronic structure upon intercalation of a full layer of Li into the interlayer region of the double sandwich and the bulk material. Donation of the Li conduction electron to the lattice causes an interesting rearrangement of the Ti-based occupancy of the valence bands.

II. COMPUTATIONAL DETAILS

A. Crystal structure and symmetry

TiS_2 crystallizes in the CdI_2 crystal structure. A projected view of the crystal structure is shown in Fig. 1. The arrangement of the Ti and S atoms within the layers is hexagonal. The stacking of the layers is *ABC-ABC-*$\cdots$, where the S atoms occupy the A and C sites and the Ti atoms occupy the B sites. The S layer is separated by $0.25c_0$ from the Ti layer in the pure material, where c_0 is the lattice constant in the z direction. Thus the intrasandwich and the intersandwich separation of the S layers are equal.[12]

Our calculation of the intercalated material is for a full layer of Li on the octahedral B sites in the intersandwich region. In this case the space group of the crystal remains unchanged. The volume of the crystal expands by 11.5% (Ref. 12) upon intercalation, most of the increase being in the z direction and most of that again being in the interlayer S-S distance, whereas the intralayer distance remains almost unchanged, as we would expect. In Table I we show the values of the crystal-structure constants and also some of the other inputs used in our calculations.[13]

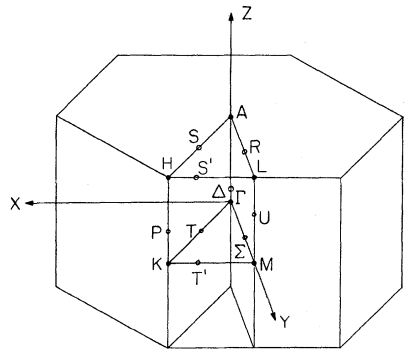

FIG. 2. Brillouin zone for the TiS_2 structure.

TABLE II. Small group of $\vec{k}$ for symmetry points in the Brillouin zone, and point-group operation used for partial symmetrization of the LAPW basis.

$\vec{k}$ points	Small group of $\vec{k}$	Operation used in symmetrization
Γ,A	D_{3d}	i
M,L	C_{2h}	i
K,H	D_3	$C_2=i\sigma$
Σ,R,U	C_{1h}	σ
T,T',S,S'	C_2	$C_2=i\sigma$
Δ	C_{3v}	σ
P	C_3	

The space group of the crystal is $D_{3d}^3(P\bar{3}m\,1)$. In Fig. 1 we have marked in the rotation axes and mirror planes of the corresponding point group $D_{3d}(\bar{3}m)$. The Brillouin zone is shown in Fig. 2 with the irreducible wedge outlined. At symmetry points that have a subgroup of order 2 linear combinations of the basis functions are formed that transform as the symmetric and antisymmetric representations, and thereby block diagonalizing the overlap and Hamiltonian matrices. In Table II we give the small group of $\vec{k}$ for the symmetry points shown in Fig. 2 and the operation used in symmetrizing the basis functions, if any. Compatibility relations deduced from the character table are useful in drawing the band structure.[13] Not only does the symmetrization of LAPW's reduce the computation time, but the resulting symmetry labels denote the interplane nodal structure essential for intepretation of level ordering and splittings.

B. LAPW band method

The linearized augmented-plane-wave (LAPW) method used in this work has been described in the literature[13]; here we only present an outline of the basic approach. A variational basis of the form

$$\phi_{i\vec{k}}(\vec{r})=\sum_{lm}[A_{lm}^{i}(\vec{k})u_l(E_l,r)+B_{lm}^{i}(\vec{k})\dot{u}_l(E_l,r)]Y_{lm}(\hat{r}) \quad (1)$$

is used to expand the Bloch functions inside spherical regions around each atom. The E_l energy parameters control the shape of the radial functions and can be given different values for each l and each atom type. The energy derivative functions $\dot{u}_l=\partial u_l/\partial E\,|_{E=E_l}$ are chosen to allow an efficient "Taylor-series" expansion of the eigenstates for energies close to E_l. The E_l are normally chosen to lie near the center of the bands of interest.

Outside the atomic muffin-tin spheres in interstitial regions, the eigenstates are expanded in plane waves. In the case of film geometry only two-dimensional periodicity holds and the interstitial LAPW's are represented as

$$\phi_{\vec{k}}^{mn}(\vec{r})=\Omega^{-1/2}e^{i\vec{K}_{mn}\cdot\vec{r}}, \quad (2)$$

where Ω is a normalizing factor, and $\vec{K}_{mn}=\vec{k}+\vec{g}_m+g_n\hat{z}$. Here $\vec{k}$ is the two-dimensional (2D) Bloch vector, $\vec{g}_m$ is a 2D reciprocal-lattice vector, and g_n labels Fourier components for the expansion in the aperiodic z direction.

The expansion coefficients A^i,B^i of Eq. (1) are obtained by matching the LAPW's and their radial derivatives across the atomic sphere boundaries. Again for film geometry, it is convenient to consider *vacuum* regions to develop an efficient expansion for $|z|>D$, where D is the film thickness. In this region we write

$$\phi_{\text{vac},\vec{k}}^{mn}(\vec{r})=[A_{mn}^{\text{vac}}(\vec{k})u_m(E_v,z)+B_{mn}^{\text{vac}}(\vec{k})\dot{u}_m(E_v,z)]e^{i\vec{k}_m\cdot\vec{r}} \quad (3)$$

in analogy with Eq. (1). The expansion bases $u_m,\dot{u}_m$ are solutions of Schrödinger's equation for the average of the full potential over the x-y plane. Depending upon the value of the vacuum energy parameter E_v, the basis function may have either damped or oscillatory behavior for large $|z|$.

The LAPW's are again matched at the vacuum-film boundary, and a secular equation is set up to determine the eigenenergies and corresponding eigenvectors for a discrete grid of $\vec{k}$ values. The wave functions of the form

$$\psi_n(\vec{k},\vec{r})=\sum_i C_{ni}(\vec{k})\phi_{i\vec{k}}(\vec{r}) \quad (4)$$

are then occupied according to Fermi statistics to generate the charge density required for self-consistent iterations. The energy spectrum $E_n(\vec{k})$ is decomposed or projected in various ways to aid in interpretation of the atomic character of the states.

C. Self-consistent crystal potential and charge density

The special $\vec{k}$ points of Chadi and Cohen[14] were used for calculating the self-consistent charge density. They are listed in Table I. For the film calculations the 3 $\vec{k}$-point set was found to yield a potential that was in surprisingly good agreement with the 6 $\vec{k}$-point set, the largest difference being less than 4 mRy. Hence, the 3 $\vec{k}$-point set was used in the self-consistency iterations. In the bulk calculations we used the 12 $\vec{k}$-point set obtained from

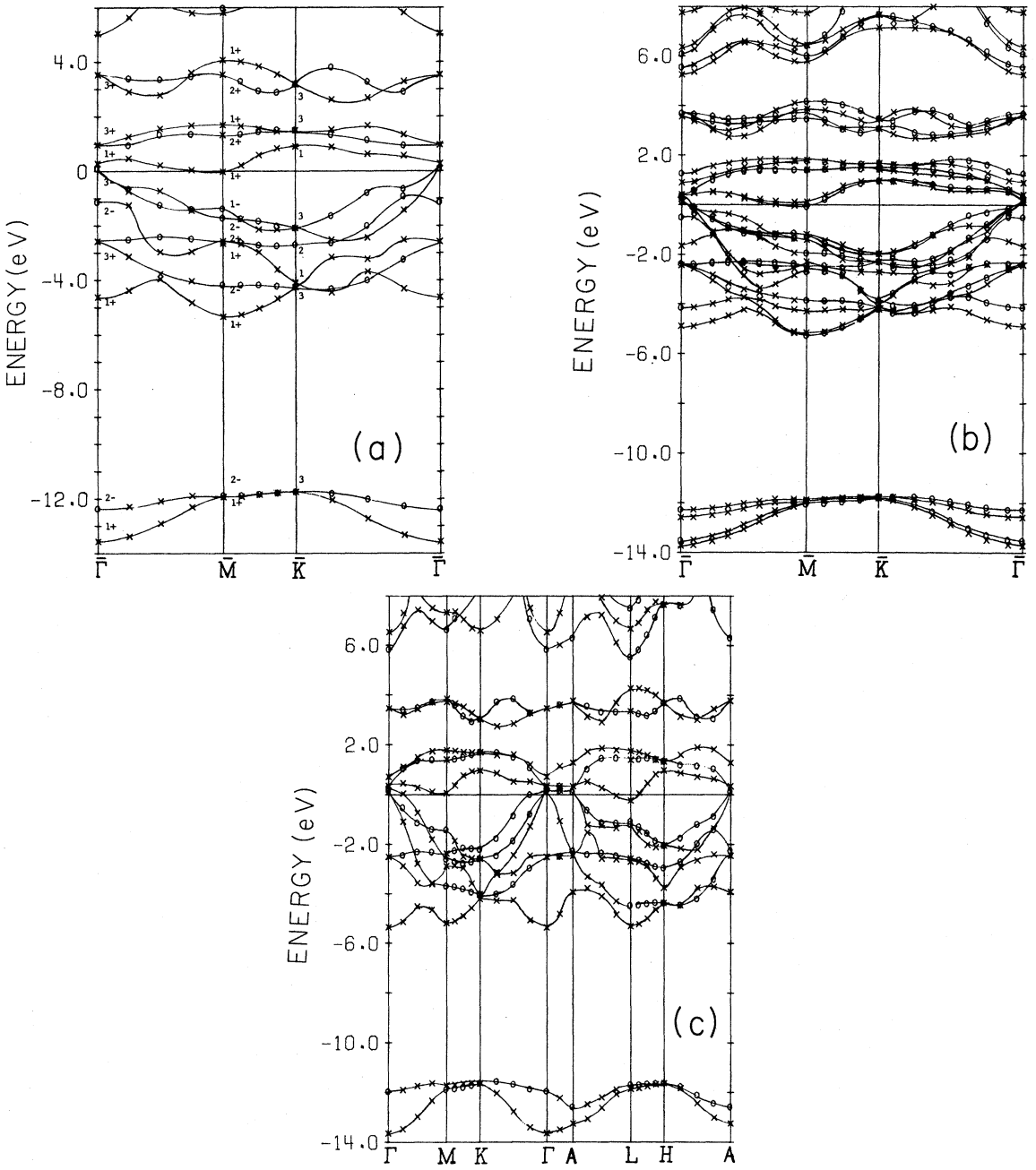

FIG. 3. Self-consistent LAPW band structures. Calculated data points for even and odd parity states with respect to the operations listed in Table II are indicated by × and ○, respectively: (a) single sandwich, S-Ti-S, (b) double sandwich, $(S\text{-}Ti\text{-}S)_2$, (c) bulk TiS_2.

Chadi and Cohen's 6 $\vec{k}$-point set for D_{6h} symmetry, since the irreducible wedge of a D_{3d} crystal is twice as large as that of a D_{6h} crystal with the same lattice constants.

The calculations are performed in the warped muffin-tin approximation, i.e., no shape approximations are made in the interstitial and vacuum regions but the potential in the atomic spheres is spherically averaged. The warping terms in the interstitial region are found to produce level shifts of as much as 1 eV, compared to levels of the uncorrected muffin-tin potential. We believe the atomic nonspherical terms that we have neglected are much less important for the following reason: A trial calculation was carried part way to self-consistency with the radius of the Ti sphere reduced

from 2.78 to 2.34 a.u., and with the radius of the S sphere increased by the same amount. The largest difference found in the eigenvalues was 0.2 eV; part of this is probably due to the fact that the calculation with the changed radii was not run all the way to self-consistency. Since the nonspherical terms would be largest at the sphere boundary, this shows that intrasphere angular terms are not very important (see, however, discussion of the S p —Ti d band gap below).

In order to produce accurate charge-density plots of the individual states useful in discussing bonding interactions, it is necessary to keep the nonspherical wave-function terms. Spherical harmonics up to $l=6$ were included in the atomic sphere regions for the wave functions, and up to $l=8$ in the charge density for this purpose. At the end of the self-consistent iterations a finer $\vec{k}$ grid was used to calculate properties so as to minimize interpolation errors. The density of states (DOS) for bulk and film were calculated by the linear tetrahedron and triangle methods,[15,16] respectively. Twenty-three $\vec{k}$ points in the irreducible triangle were used for the film calculations and a uniform mesh of 75 $\vec{k}$ points in the irreducible wedge was used for the bulk calculations.

III. BAND STRUCTURE AND DENSITY OF STATES

A. Level structure and bonding

In Figs. 3(a)—3(c) we give the band structure of (a) the single sandwich S-Ti-S, (b) the double sandwich $(\text{S-Ti-S})_2$, and (c) bulk TiS_2. The zero of the energy is chosen to be at the Fermi level E_F. The two low-lying bands are S 3s-like, the six bands (twelve for the double sandwich) lying almost entirely below the Fermi energy are S p-like, and the five bands lying almost entirely above E_F are Ti 3d-like, though there is considerable admixture in some of the states as will appear further in the partial densities of states. The nearest S atoms form an approximately regular octahedron around the Ti atoms. Hence the d bands split into a t_{2g}-like triplet and an e_g-like doublet of subbands, as one would expect from crystal-field theory.

If we were to start with two sandwiches far apart from each other we would have a pair of degenerate levels for each level in the single sandwich. If the two sandwiches are brought closer to each other the levels will split and the extent to which they split is a measure of the intersandwich interaction. Similarly, to compare with the bulk structure, we may start with an infinite number of sandwiches far apart from each other; we then have an additional quantum number k_z that is not present in the single sandwich. States with all values of k_z will be degenerate, i.e., there will be no dispersion of the bands along the z direction. On bringing the sandwiches closer to each other this degeneracy is lifted; thus the band dispersion in the z direction is a measure of the intersandwich interaction.

We can make the following correspondence between the single sandwich levels at the zone center $\bar{\Gamma}$ and the double sandwich and bulk levels:

Single sandwich	Double sandwich	Bulk
$\bar{\Gamma}_{1+}$	$\bar{\Gamma}_{1+}$ and $\bar{\Gamma}_{2-}$	Γ_{1+} and A_{1+}
$\bar{\Gamma}_{2-}$	$\bar{\Gamma}_{2-}$ $\bar{\Gamma}_{1+}$	Γ_{2-} A_{2-}
$\bar{\Gamma}_{3+}$	$\bar{\Gamma}_{3+}$ $\bar{\Gamma}_{3-}$	Γ_{3+} A_{3+}
$\bar{\Gamma}_{3-}$	$\bar{\Gamma}_{3-}$ $\bar{\Gamma}_{3+}$	Γ_{3-} A_{3-}

We illustrate this with a simple example, the S 3s states. In a single sandwich these give rise to a $\bar{\Gamma}_{1+}$ and a $\bar{\Gamma}_{2-}$ [see Fig. 3(a)]; the phase of the wave function with respect to adjacent layers can be schematically represented as $\overset{+}{+}$ and $\overset{+}{-}$, respectively. In the double sandwich [Fig. 3(b)] each of these gives rise to a $\bar{\Gamma}_{1+}$ and a $\bar{\Gamma}_{2-}$ and in the bulk [Fig. 3(c)] they give rise to a continuum of levels along the Γ-A direction. We visualize the interplane nodal structure from the following diagrams, keeping in mind that the unit cell of the double sandwich has two formula units and in the bulk there is one formula unit per unit cell, while k_z represents the change in phase from one unit cell to the next in the z direction:

$$\begin{array}{ccccccccc}
+ & & \left\{\begin{array}{cc} + & + \\ + & + \end{array}\right. & & + & & \left\{\begin{array}{cc} + & + \\ - & - \end{array}\right. & \\
 & \rightarrow & & & & \rightarrow & & & \\
+ & & \left\{\begin{array}{cc} + & - \\ + & - \end{array}\right. & & - & & \left\{\begin{array}{cc} + & - \\ - & + \end{array}\right. & \\
\bar{\Gamma}_{1+}\text{(single)} & & \bar{\Gamma}_{1+} & \bar{\Gamma}_{2-}\text{(double)} & \bar{\Gamma}_{2-}\text{(single)} & & \bar{\Gamma}_{2-} & \bar{\Gamma}_{1+}\text{(double)} & \\
 & & \Gamma_{1+} & A_{1+}\text{(bulk)} & & & \Gamma_{2-} & A_{2-}\text{(bulk)} &
\end{array}$$

TABLE III. Energy levels of single sandwich TiS_2 at $\bar{\Gamma}$ and corresponding levels of double sandwich and bulk. Energies are given relative to E_F in eV.

Predominant atomic character	TiS_2 single sandwich State	Energy	$(TiS_2)_2$ double sandwich State	Energy	Diff.[a]	TiS_2 bulk State	Energy	Diff.[b]
S $3s$	$\bar{\Gamma}_{1+}$	−13.55	$\bar{\Gamma}_{1+}$	−13.71	0.21	Γ_{1+}	−13.57	0.40
			$\bar{\Gamma}_{2-}$	−13.50		A_{1+}	−13.17	
S $3s$	$\bar{\Gamma}_{2-}$	−12.36	$\bar{\Gamma}_{1+}$	−12.57	0.31	A_{2-}	−12.51	0.62
			$\bar{\Gamma}_{2-}$	−12.26		Γ_{2-}	−11.89	
S $3p_z$	$\bar{\Gamma}_{1+}$	−4.62	$\bar{\Gamma}_{1+}$	−4.87	0.73	Γ_{1+}	−5.23	1.45
			$\bar{\Gamma}_{2-}$	−4.14		A_{1+}	−3.83	
S $3p_{xy}$	$\bar{\Gamma}_{3+}$	−2.58	$\bar{\Gamma}_{3+}$	−2.42	0.04	Γ_{3+}	−2.43	0.06
			$\bar{\Gamma}_{3-}$	−2.38		A_{3+}	−2.37	
S $3p_z$	$\bar{\Gamma}_{2-}$	−1.13	$\bar{\Gamma}_{1+}$	−1.64	1.14	A_{2-}	−2.13	2.43
			$\bar{\Gamma}_{2-}$	−0.50		Γ_{2-}	0.25	
S $3p_{xy}$	$\bar{\Gamma}_{3-}$	0.09	$\bar{\Gamma}_{3+}$	0.11	0.06	A_{3-}	0.18	0.16
			$\bar{\Gamma}_{3-}$	0.17		Γ_{3-}	0.34	
Ti $3d$	$\bar{\Gamma}_{3+}$	0.28	$\bar{\Gamma}_{3-}$	0.37	0.05	A_{3+}	0.42	0.01
			$\bar{\Gamma}_{3+}$	0.42		Γ_{3+}	0.43	
Ti $3d$	$\bar{\Gamma}_{1+}$	0.97	$\bar{\Gamma}_{1+}$	0.91	0.36	Γ_{1+}	0.79	0.57
			$\bar{\Gamma}_{2-}$	1.27		A_{1+}	1.36	
Ti $3d$	$\bar{\Gamma}_{3+}$	3.53	$\bar{\Gamma}_{3+}$	3.57	0.12	Γ_{3+}	3.53	0.32
			$\bar{\Gamma}_{3-}$	3.69		A_{3+}	3.85	

[a]Splitting between interlayer bonding and antibonding levels.
[b]k_z dispersion in bulk bands.

In Table III we give the energy levels of the single sandwich at $\bar{\Gamma}$ and the corresponding levels of the double sandwich and the bulk. The splittings within pairs originating from the same state in the single sandwich are seen to be small in most cases. Two states do have a fairly large splitting of 0.7 and 1.1 eV in the double sandwich and 1.4 and 2.4 eV in the bulk. The predominant atomic character of the states was determined by integrating the l-component charge densities within the atomic spheres, and by examining wave-function contour maps. These states are of S p_z character, the very states we would expect to extend the furthest into the intersandwich region, and which had been identified by Mattheiss[17] as the critical states for interlayer interactions. Very recently Benesh and Woolley have called attention to the effects of shifts in the bulk Γ_{2-} state due to applied pressure.[18]

The dispersion of the bulk bands in the Γ-A direction is approximately double the splitting of the bands at $\bar{\Gamma}$ in the double sandwich. In fact, it is interesting to note that the single-sandwich bands are approximately the average of the bulk bands along the ΓMK and the ALH directions and the double-sandwich bands are similar to those obtained by superposing the bulk bands from planes one-quarter and three-quarters of the way up from the ΓMK and the ALH planes.

It is not always possible to make a clear distinction between bonding and antibonding states in anything more complicated than a linear molecule, but it is often possible to make qualitative arguments in terms of these concepts. We have found that it is possible to characterize all the occupied single-particle states at Γ and A as being either bonding or antibonding states in the intrasandwich and intersandwich S−S bond directions, with the Ti atoms merely mediating the interaction. With the use of these concepts it is possible to explain many of the features of the band structure of TiS_2 and some of the changes that occur upon intercalation.

From the schematic diagrams just given we see that the bulk Γ_{1+} and the A_{1+} states have bonding character in the *intra*sandwich region, whereas the Γ_{2-} and the A_{2-} are antibonding in this region. The Γ_{1+} and the A_{2-} are bonding in the *inter*sandwich region, whereas the Γ_{2-} and the A_{1+} are antibonding in this region. When we examine the charge density of individual states we see that although the intrasandwich and the intersandwich distances are equal, there is appreciably more

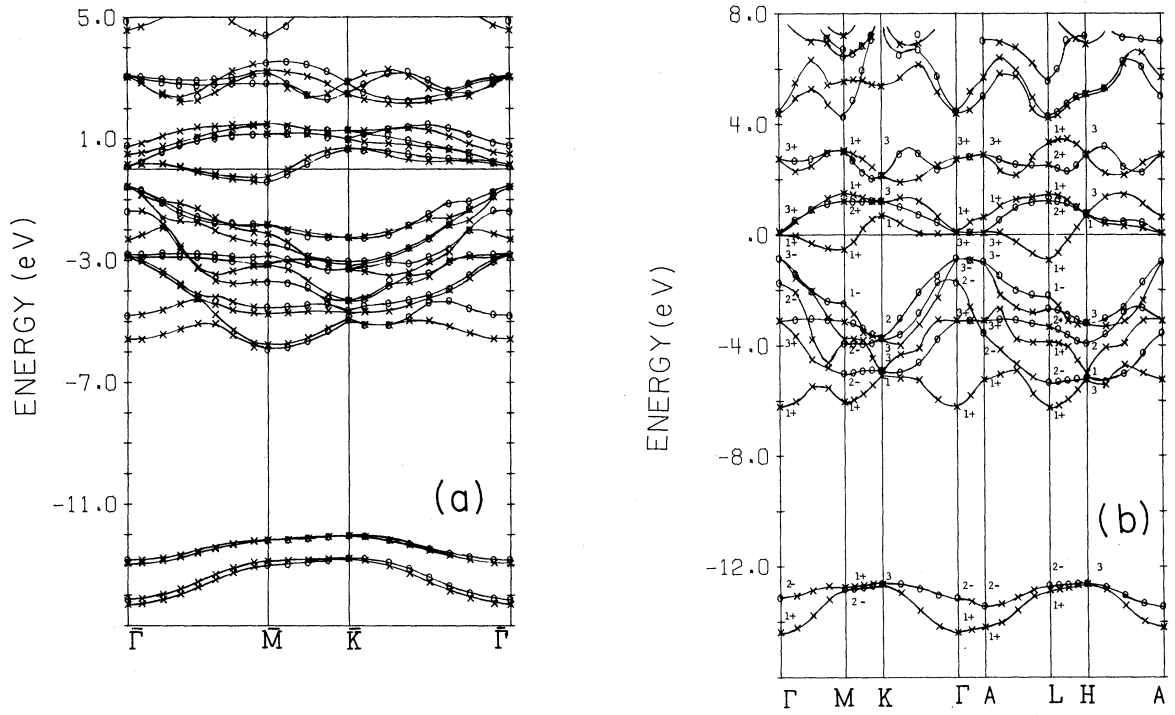

FIG. 4. Self-consistent LAPW band structures. Calculated data points for even and odd parity states with respect to the operations listed in Table II, are indicated by × and ○, respectively. (a) Intercalated sandwich (S-Ti-S)-Li-(S-Ti-S), (b) bulk $LiTiS_2$, intercalated structure.

charge in the intrasandwich S—S bond than in the intersandwich S—S bond. On the basis of the usual overlap arguments, this confirms our expectation that the intrasandwich bonds are stronger than the intersandwich bonds. This being so we would predict that the states derived from some particular atomic orbitals would be in order of increasing energy $\Gamma_{1+} < A_{1+} < A_{2-} < \Gamma_{2-}$. From Fig. 3 and Table III we see that this is true in all cases. Further, we would predict that an increase in the intrasandwich S-S distance would reduce both the Γ_{1+}-Γ_{2-} and the A_{1+}-A_{2-} splittings, whereas an increase in the intersandwich S-S distance would reduce the Γ_{1+}-Γ_{2-} splitting but increase the A_{1+}-A_{2-} splitting. Upon intercalation, the intrasandwich and the intersandwich distances between the S planes increase by 1% and 16.5%, respectively. Both these changes act to decrease the Γ_{1+}-Γ_{2-} splitting but they have opposite effects on the A_{1+}-A_{2-} splitting. Comparing the pure TiS_2 results of Fig. 3 with the Li-intercalated results given in Fig. 4, we see that indeed the calculated Γ_{1+}-Γ_{2-} splittings are considerably reduced, whereas there is a slight increase in the A_{1+}-A_{2-} splitting.

B. Band features and optical properties

The question whether stoichiometric TiS_2 is semiconducting or semimetallic has been a matter of great controversy. It was originally classified as a semiconductor.[2,19] Some years ago most experimentalists believed that it was semimetallic,[20–23] but the prevalent opinion now is that stoichiometric TiS_2 is semiconducting[24–26] and that the observed semimetallic properties are due to excess Ti.

Table IV compares some calculated and experimentally determined band features of TiS_2 obtained by several authors. Our calculations are in fair agreement with experiment and in good agreement with the linear combination of atomic orbitals—discrete variational method (LCAO-DVM) results of Zunger and Freeman[10] with the exception of the value of the *p-d* gap. We calculate a *semimetal* with an indirect $\bar{\Gamma}$-$\bar{M}$ overlap of 0.1 and 0.2 eV in the single and double sandwiches, respectively, and an indirect Γ-L overlap of 0.5 eV in the bulk. It is worth mentioning here that Mattheiss[17] has observed that inclusion of the nonspherical terms in the muffin-tin spheres,

TABLE IV. Comparison of calculated and experimentally determined band features of TiS_2. Energies in eV. (1) Semiempirical LCAO (Ref. 7), (2) non-self-consistent Korringa-Kohn-Rostoker method (Ref. 8), (3) self-consistent OPW (Ref. 9), (4) self-consistent LCAO-DVM (Ref. 10), and (5) LCAO (Ref. 11).

	Experiment	(1)	(2)	(3)	(4)	(5)	Present work
Width of S s band	2−3[a],1−2[b]			2.5	2.0	2.6	2.0
Width of S p band	6−7[a],4−4.5[b] 6−7[c]	2.9	5.0	6.6	5.5	6.1	5.6
Width of Ti d band	4[d]	2.1	2.6	7.1	4.4	3.3	4.5
S s−S p gap	6−7[b]			5.5	6.8	5.9	6.3
S p−Ti d gap	0.2−0.3[e]	0.8	2.0−2.7	1.5	0.2	0.7	−0.5
t_{2g}-e_g splitting	2.2[d],2.1[c]	1.4	1.3	t_{2g},e_g are not distinct	2.3	2.0	2.6

[a]He photoemission, Ref. 32.
[b]X-ray photoelectron spectra, Ref. 33.
[c]Appearance potential spectra, Ref. 34.
[d]X-ray emission and absorption, Ref. 20.
[e]See text.

which we have neglected, caused the p-d band gap in another transition-metal dichalcogenide $NbSe_2$ to increase by 0.3 eV. This shift is in the right direction but is not large enough to bring our band structure into agreement with experimental evidence. Our LAPW calculations are semirelativistic,[13] i.e., the main level shifts due to relativistic effects are included self-consistently. Spin-orbit splittings of a few tenths eV are expected in a full relativistic treatment; it would be interesting to know whether this is sufficient to "open the gap" again.[27]

The optical reflectivity[19] and the optical transmission coefficient[21,28] of TiS_2 have been measured. The reflectivity has been measured in the energy range from 0−12 eV and shows much structure. Unfortunately, it has not been transformed (extrapolation of the high-energy region would be necessary) to obtain the absorption coefficient, which is the quantity that can be most directly calculated. The optical transmission of nearly stoichiometric thin films was measured from about 0.5 to 3.5 eV by Perry[21] revealing a semimetal with a sharp onset of absorption at 1.03 eV with additional structure at ~1.5, 2.1, 3.2, and 3.4 eV. The results are qualitatively similar to those obtained by Beal *et al.* on highly nonstoichiometric samples. Free-carrier absorption is observed in the infrared region.

A theoretical calculation of the absorption coefficient would involve evaluating the matrix elements of the operator $\hat{\epsilon}\cdot\nabla e^{i\vec{k}\cdot\vec{r}}$ where $\vec{k}$ is the wave vector of the photon and $\hat{\epsilon}$ is its polarization. We have not evaluated the matrix elements; however, structure in the absorption spectrum can at times be correlated with direct transitions at high-symmetry points. The bands must have zero slope at some high-symmetry points and therefore are parallel there, giving large DOS contributions. In Table V we give the dipole-allowed transitions from the S s,p bands to the Ti d bands. Since current experimental evidence seems to favor the interpretation that stoichiometric TiS_2 is a semiconductor with a band gap of 0.2−0.3 eV, we have shifted the calculated Ti d bands up by 0.75 eV to make quantitative comparisons. In Fig. 5 we present a histogram of the allowed transitions for $\vec{E}||x$ or y polarization since the experiments are performed with unpolarized light incident perpendicularly to the x-y plane. Our results show that the edge noted at ~1.0 eV is probably due to direct transitions at Γ and A regions of the Brillouin zone (BZ). The shoulder at 1.6 eV is represented by the beginning of transitions around the L point. The strong peak at ~2.2 eV represents the point where M transitions begin, but it is likely that large regions of the BZ also contribute to the transitions in this energy range. The shoulders at 3.2−3.3 eV observed at the extreme end of the measured transmission spectra are seen to be the beginning of a very intense band spanning from ~3.2−7 eV. Electron-energy-loss experiments would be useful to resolve this major feature of the electronic structure.

TABLE V. Dipole-allowed optical transitions in bulk TiS_2 from S s,p bands to Ti d bands at four high-symmetry $\vec{k}$ points. The Ti d bands have been shifted up by 0.75 eV relative to the S s,p bands. Energies are in eV.

k point	irred. rep.	Polarization	
		$\vec{E}\|\|x$ or y	$\vec{E}\|\|z$
Γ	$2^-\rightarrow1^+$		1.30,13.44
	$2^-\rightarrow3^+$	0.93,4.04,13.07,16.17	
	$3^-\rightarrow3^+$	0.84,3.94	0.84,3.94
	$3^-\rightarrow1^+$	1.30	
A	$2^-\rightarrow1^+$		4.29,14.62
	$2^-\rightarrow3^+$	3.34,6.77,13.68,17.14	
	$3^-\rightarrow3^+$	0.98,4.41	0.98,4.41
	$3^-\rightarrow1^+$	1.93	
		$\vec{E}\|\|x$	$\vec{E}\|\|y$ or z
M	$1^-\rightarrow1^+$	2.23,3.95,6.01	
	$1^-\rightarrow2^+$		3.57,5.88
	$2^-\rightarrow1^+$		2.23,3.95,4.49,6.01,6.21
			8.27,12.7,14.42,16.48
	$2^-\rightarrow2^+$	4.75,5.83,7.06,8.14	
		14.04,16.35	
L	$1^-\rightarrow1^+$	1.72,3.7,6.23	
	$1^-\rightarrow2^+$		3.35,5.31
	$2^-\rightarrow1^+$		1.6,3.58,4.98,6.11,6.97
			9.49,12.23,14.21,16.74
	$2^-\rightarrow2^+$	3.23,5.19,6.61,3.57,	
		13.85,15.81	

C. Comparison with intercalated structure

A semiempirical LCAO calculation of the energy bands of Li-TiS_2 has been made by McCanny.[29] McCanny finds that the following changes occur upon intercalation: (i) The S 3s bands move down to lower energies and are split apart further at Γ. (ii) Some bands, particularly the S p_z-like bands, have a smaller dispersion along Γ-A. (iii) There is an increase of about 0.8 eV in the S p – Ti d gap. (iv) A state that lies above the Ti 3d-like states in pure TiS_2 is pulled down in energy at Γ by about 7 eV into the Ti 3d band region.

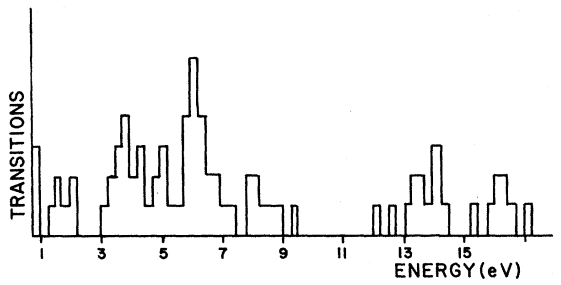

FIG. 5. Optical absorption of TiS_2, estimated from joint density of states due to dipole-allowed transitions.

Our calculations confirm some of these changes but disagree with others. We find that the S 3s and 3p bands move down in energy by ~0.7 eV relative to the Ti 3d-t_{2g} bands; the Ti 3d-e_g bands also move down relative to the Ti 3d-t_{2g} bands but by a smaller amount, ~0.3 eV. As discussed before we obtain a decrease in the Γ-A dispersion in agreement with McCanny and our bonding argument based upon the lattice expansion. The Γ_{1+}-Γ_{2-} splitting is found to decrease in agreement with our prediction, but in disagreement with McCanny's results. Comparing Figs. 3(c) and 4(b) we see that high-lying states are pulled down by about 1.5 eV relative to the Ti 3d-e_g bands but that this shift is not large enough for the band to intersect the Ti 3d bands, as McCanny finds. Aside from these shifts the band structures of the stoichiometric and lithiated films are indeed very similar. There is no evidence of the formation of additional "Li-bonding" bands in the valence region, supporting the simple idea of charge donation to form Li^+ upon intercalation. However, we can see from the relative band-structure shifts, and from analysis of the charge density, that the rigid-band model is an oversimplification.

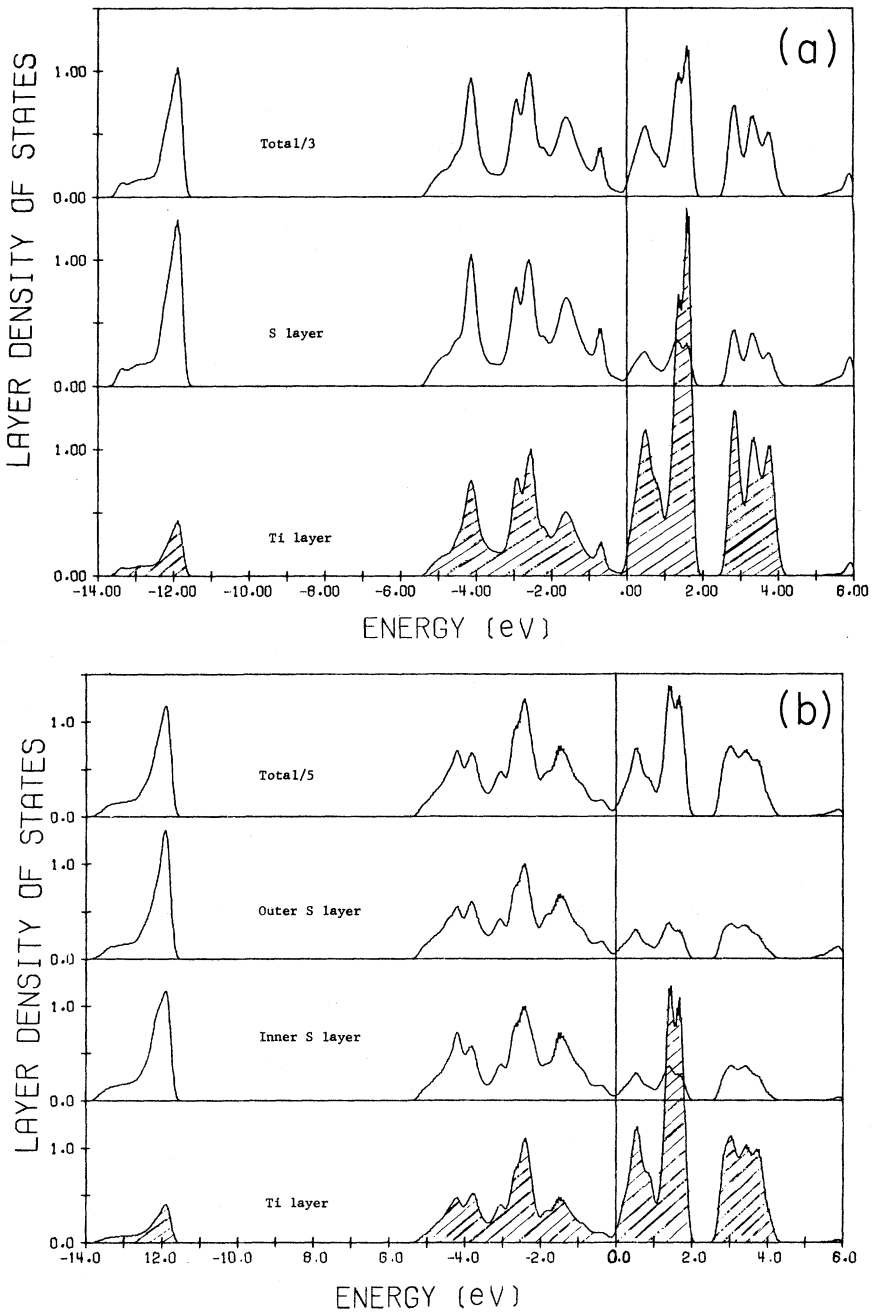

FIG. 6. Layer projected density of states, in units of states per (eV spin). (a) Single sandwich, TiS_2, (b) double sandwich, $(TiS_2)_2$, (c) bulk TiS_2.

In Figs. 6(a)—6(c) we show the layer projected density of states for TiS_2 films and bulk, broadened by convolution with a Gaussian of width 0.2 eV, in the same sequence as the bands in Fig. 3. In most metallic materials the DOS obtained from a thin-film calculation are considerably narrower than the bulk DOS because there are fewer neighbors with which to interact.[30] The similarity of the single-sandwich, double-sandwich, and bulk DOS seen in Figs. 6(a)—6(c) is indicative of relatively weak intersandwich interaction, and thus of the quasi-two-dimensional nature of the electronic structure. In particular, we note that although the inner and the outer S atoms in the dou-

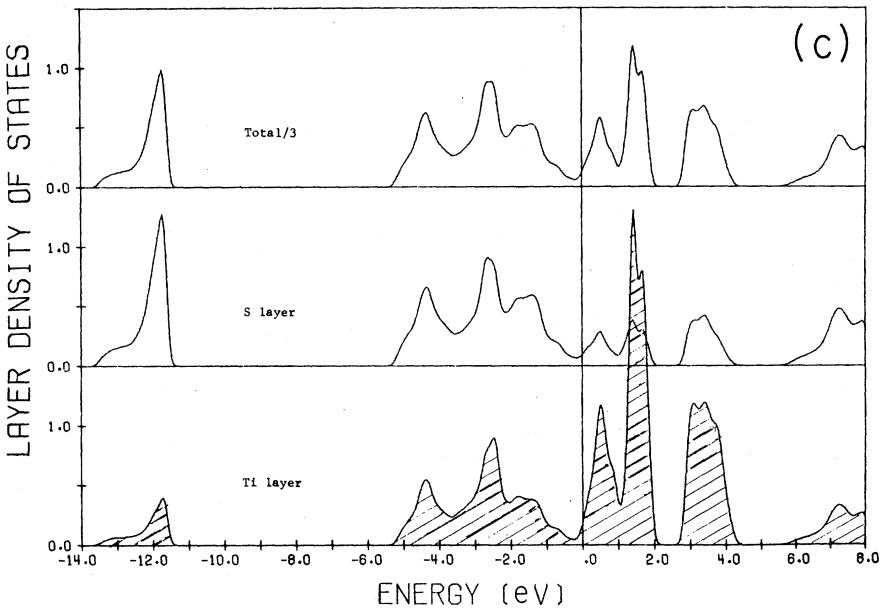

FIG. 6. (*Continued.*)

ble sandwich are inequivalent they have nearly the same DOS. In all cases we note the sizable participation of Ti $3d4sp$ states in the occupied valence-band region, clearly indicating shortcomings of the fully ionic Ti^{4+}, S^{2-} bonding models. The t_{2g} and e_g subbands are nevertheless seen as expected in the region just above E_F. Splitting of the t_{2g} band into two subbands is seen even in the single layer, and is thus a feature of the intrasandwich bonding.

The DOS of the intercalated double sandwich, shown in Fig. 7(a), reveals a difference between inequivalent sulfur layers. The states that have most of their weight on the inner S atoms are lower in energy by about 0.7 eV than those with most of their weight on the outer atoms, clearly a result of the attractive Li-site potentials. In the bulk material all S sites are equivalent; however, an experimental technique that is sensitive to both the surface and the bulk should be able to detect the upward shift of the S s and p bands on the surface atoms. Chemical shift measurements on S core states in stoichiometric versus lithiated materials would provide similar information.

In order to display the Ti—S bonding in bulk TiS_2 and the distribution of Li character in the intercalated materials, we present the layer decomposition of charge for states at Γ, near the Fermi energy, in Table VI. This table, along with Fig. 7, makes it clear that the Li contributions to the spectral density are spread across both chalcogen and metal valence and conduction bands.

IV. CHARGE DENSITY

In Fig. 8 we show the charge density of the 16 valence electrons (Ti $1s,2s,2p,3s,3p$ and S $1s,2s,2p$ states were included in the core) of bulk TiS_2: (a) in the y-z plane through the atoms in the unit cell, (b) in the x-y plane through the Ti atoms, and (c) in the x-y plane halfway between the sandwiches (empty octahedral site at the center). Figure 9(a) shows the same plot for the 17 valence electrons of bulk Li-TiS_2. From Fig. 9 we notice that the charge density is highest around the S atoms. Since the occupied valence levels are of mostly S s or S p character, with nominal valence state S^{2-}, this is to be expected. The charge around the Ti atom in TiS_2 shows some noticeable angular polarization, but in Li-TiS_2 it is considerably more spherical. In both cases there is a clear qualitative difference compared to the orthogonalized-plane-wave (OPW) results[9] of von Boehm *et al.* The present LAPW densities exhibit metal-ligand charge sharing consistent with a mixed covalent-ionic bonding structure, while the OPW densities appear to represent a purely ionic structure. The midpoint of the intrasandwich S—S bond is at the midpoint of the side edges of the contour plots (point A) and the midpoint of the intersandwich S—S bond is at the top right or the bottom left corners of the plots (point B). As mentioned before we see that even in the unintercalated materials, where the intrasandwich and the intersandwich

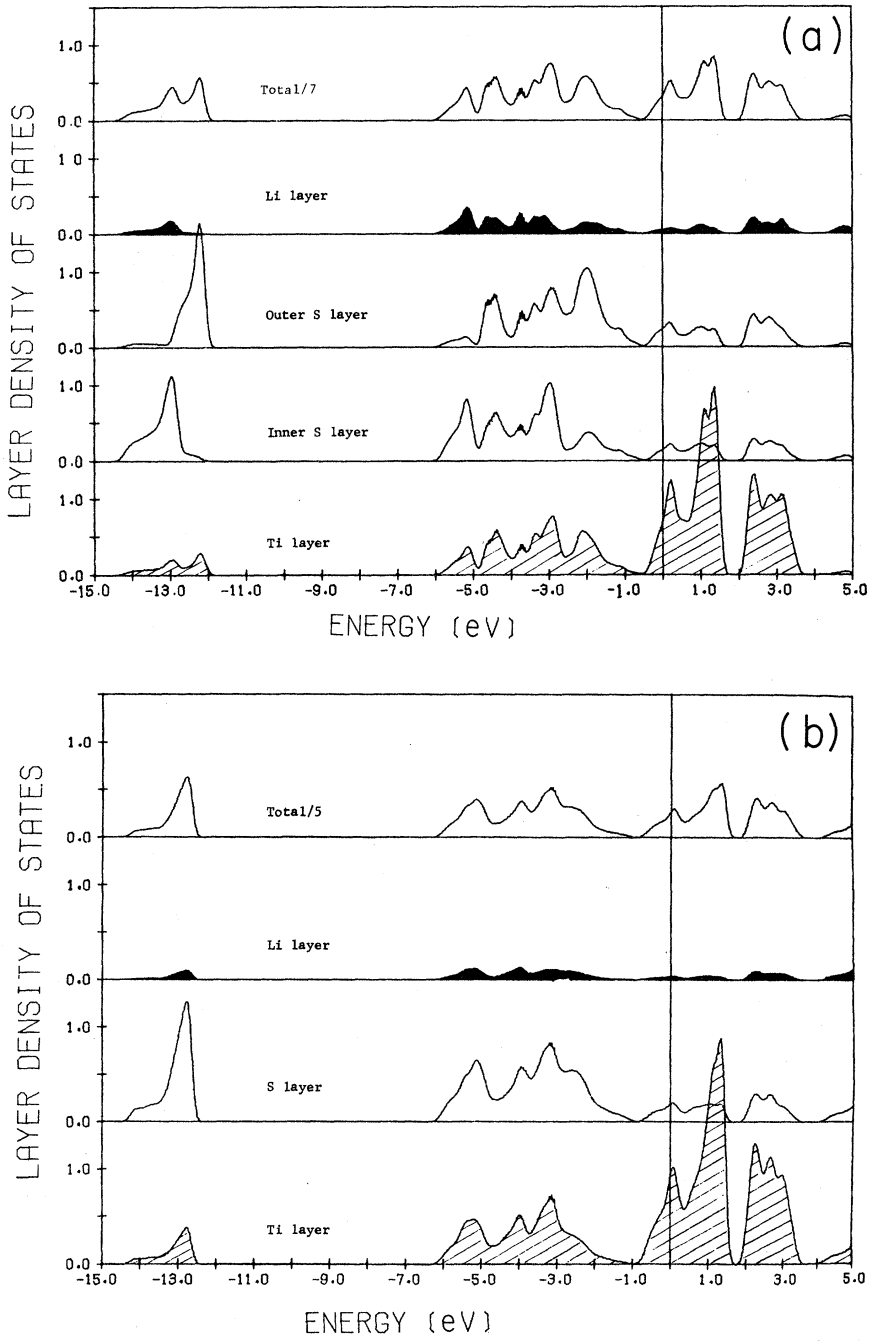

FIG. 7. Layer projected density of states, in units of states per (eV spin). (a) Intercalated sandwich, (b) bulk $LiTiS_2$.

S—S distances are equal, there is appreciably more charge in the intrasandwich bond than in the intersandwich bond.

The charge density in the x-y plane through the Ti atoms, except for the region close to the atom site, is surprisingly uniform in both materials. That is, there are regions of conduction-electron-like density not found in ionic bonded compounds. This emphasizes again the complex mixed-bonding character of the transition-metal chalcogenides similar to that found for the oxides.

Except for a very narrow peak around the Li site, and the reduced Ti polarization, the introduction of Li into the intersandwich region has affect-

TABLE VI. Layer decomposition of selected states for bulk TiS_2 and $LiTiS_2$. Energies are given relative to E_F in eV.

	TiS_2			$Li\text{-}TiS_2$			
		Fraction of charge in layer			Fraction of charge in layer		
State	Energy	Ti	S	Energy	Ti	S	Li
Γ_{1+}	−13.57	0.17	0.83	−14.05	0.15	0.77	0.06
Γ_{2-}	−11.89	0.09	0.91	−12.81	0.07	0.86	0.05
Γ_{1+}	−5.27	0.41	0.58	−5.88	0.38	0.37	0.21
Γ_{3+}	−2.43	0.49	0.50	−2.77	0.43	0.55	0.01
Γ_{2-}	+0.24	0.24	0.75	−1.41	0.22	0.59	0.18
Γ_{3-}	+0.33	0.06	0.93	−0.53	0.06	0.88	0.04

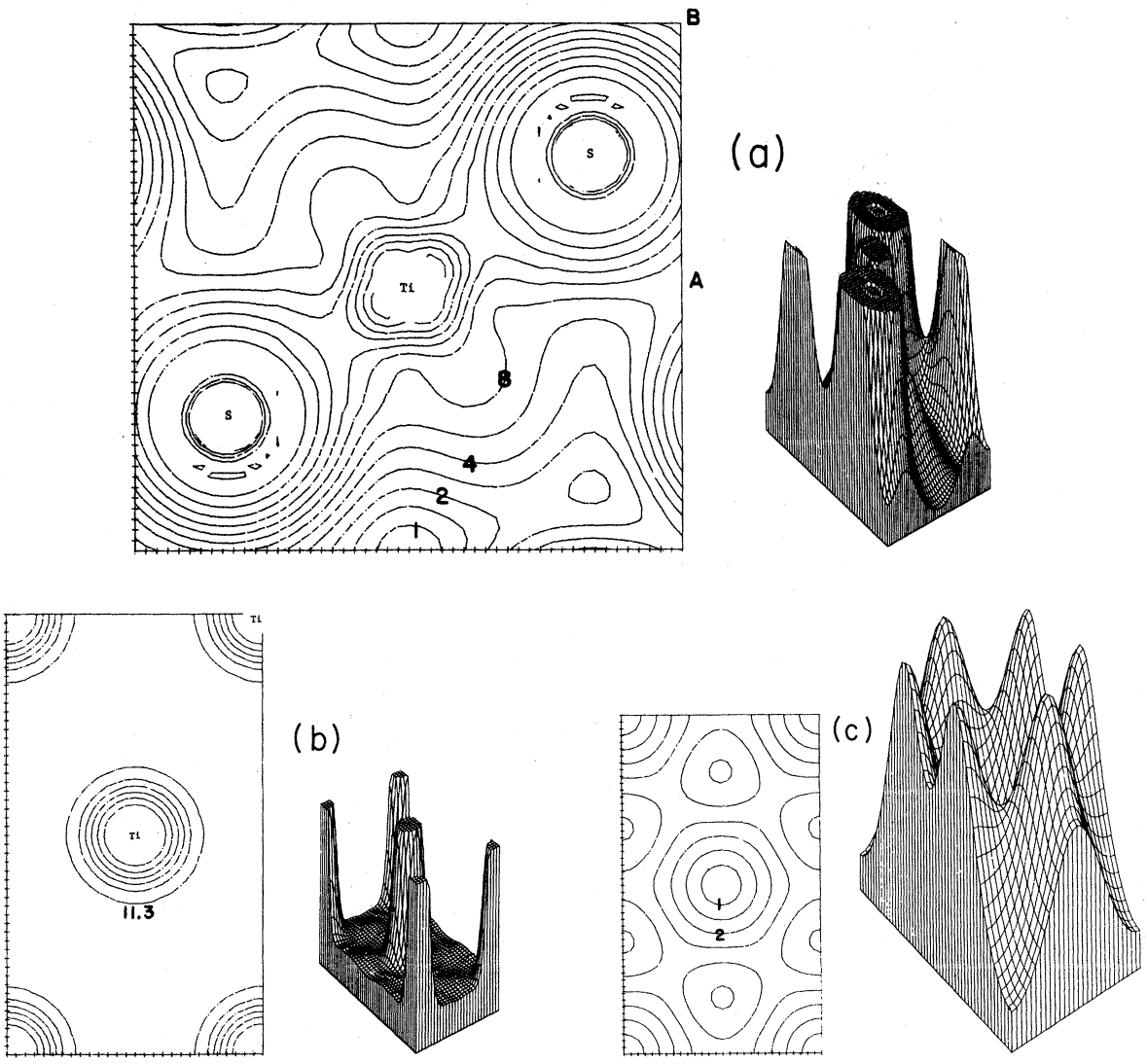

FIG. 8. Valence electron charge density for bulk TiS_2 (contour levels differ by a factor of $\sqrt{2}$), in units of electrons per unit cell. (a) y-z plane including atoms of unit cell, (b) x-y plane through Ti atoms, (c) x-y plane halfway between sandwiches.

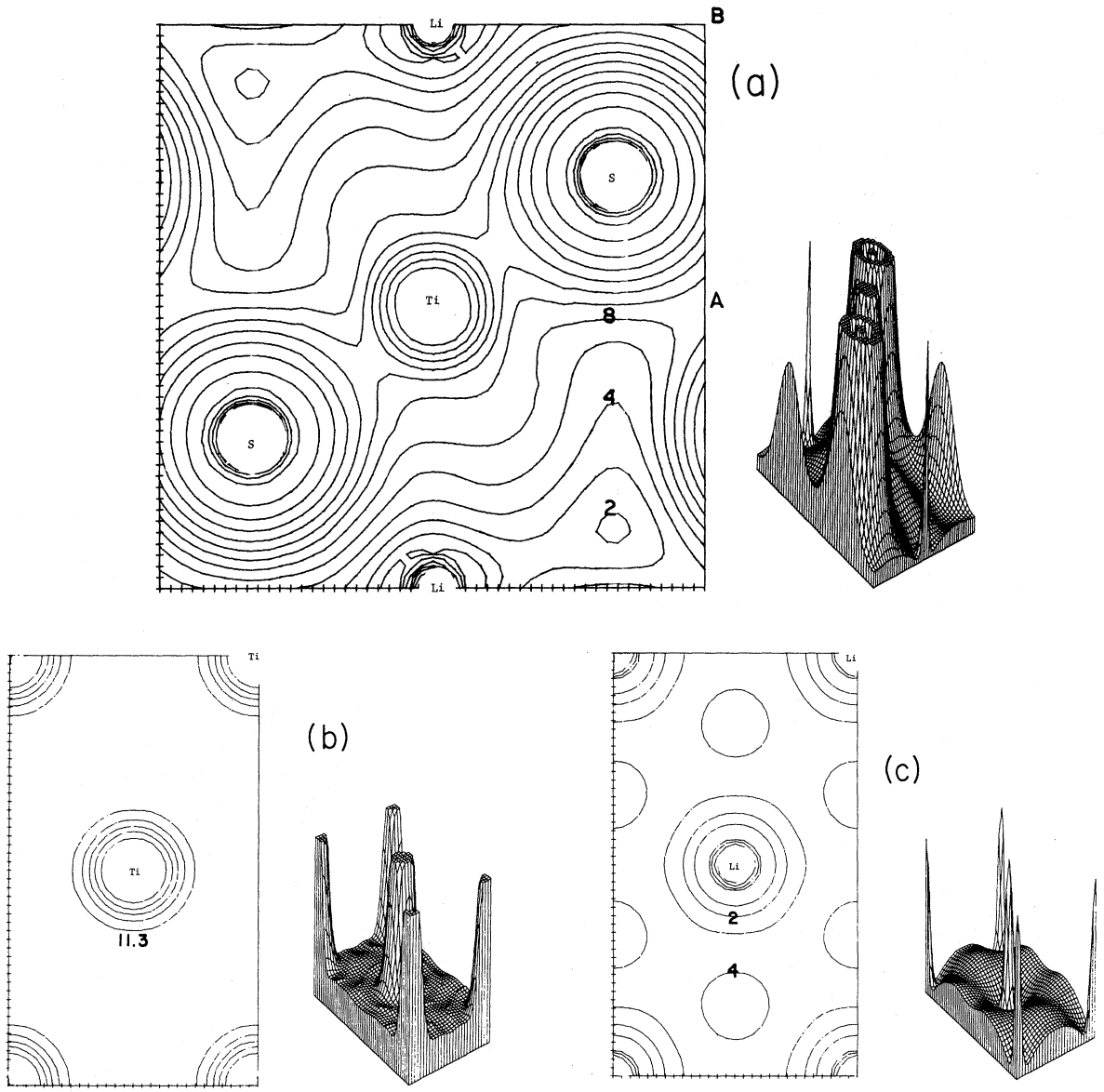

FIG. 9. Valence electron charge density for the intercalation compound $LiTiS_2$ (contour levels differ by a factor of $\sqrt{2}$), in units of electrons per unit cell. (a) y-z plane including atoms of unit cell, (b) x-y plane through Ti atoms, (c) x-y plane through Li sites, midway between sandwiches.

ed the shape of the density contours very little. In order to obtain a better idea of the redistribution of charge upon intercalation we have plotted the charge density averaged over the x-y plane, $\rho_\perp$, as a function of z in Fig. 10,

$$\rho_\perp(z)=A^{-1}\int_A \rho(\vec{r})dx\,dy\ .$$

The additional charge due to intercalation is seen to lie primarily between the Li and the S planes. This is at first a very surprising result since the additional electron "donated" by Li occupies a band that is predominantly Ti $3d$-like. We find that this charge is compensated in that the other valence states relax in such a way as to transfer part of their charge away from the Ti layer. We have studied the effect of intercalation on the fraction of the charge in layers associated with each atom type, the layer boundaries being defined to lie halfway between the planes containing atoms of a given type. We have found a shift in the charge

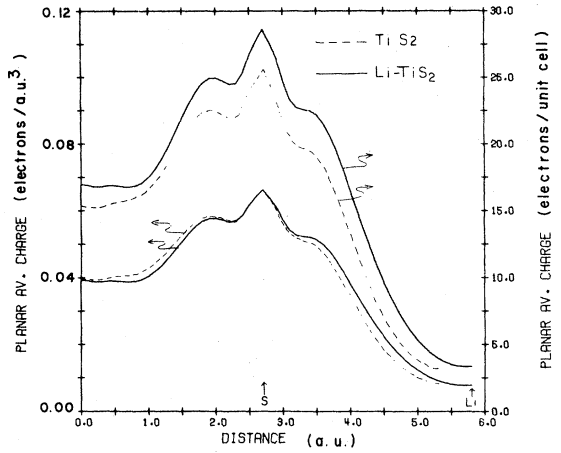

FIG. 10. Charge density averaged over x-y plane and plotted vs z.

away from the Ti layer to occur for all the *occupied* states studied throughout the Brillouin zone. In Table VI the layer weights for a few states are shown for bulk TiS_2 and bulk Li-TiS_2 in order to display this relaxation of the occupied orbitals.

V. CONCLUSIONS

The band structures and DOS of TiS_2 were calculated for a single sandwich of the material, a double sandwich, and the bulk. The similarity of the DOS of the three systems indicates weak intersandwich bonding; at the zone center Γ we can identify the two states, dominantly of S p_z character, that interact appreciably across the intersandwich region. The band structure and DOS of a double film with a full intercalated layer of Li and of the bulk-lithiated material were also calculated. Upon intercalation the S s and p bands move down in energy by about 0.7 eV and the Ti d-e_g bands move down by about 0.3 eV relative to the Ti d-t_{2g} bands. Many features of the band structure of TiS_2 and some of the changes upon intercalation can be explained by making simple arguments concerning the bonding or antibonding character of states in the intrasandwich and intersandwich S—S bond directions. Our semirelativistic LAPW band results predict that both thin-film and bulk TiS_2 are semimetallic with a band overlap of 0.5 eV in the bulk.

Contour plots of the valence charge density were presented and used to characterize general features of the bonding. None of the occupied levels has dominant Li character, according to a state-by-state analysis. The additional charge of the "Li electron" is not localized around the Li atom but is spread out in the region between the Li and the S layers, consistent with ideas of the character of the mobile Li^+ ion in this material derived from NMR and other measurements.[31]

After this work was completed we became aware of the angle-resolved photoemission experiments of Chen *et al.* on $TiSe_2$ and TiS_2.[35] The uppermost sulfur p band of TiS_2 that they observe comes close to E_F at Γ but does not cross E_F. From this they conclude that TiS_2 is a semiconductor. However, they also find an appreciable filling of a Ti d band near M and L. It is possible to have completely filled sulfur p bands and a partially filled Ti d band only if the sample contains excess Ti. However, the authors claim that their sample is stoichiometric to better than 0.5%. Hence, it seems possible that the experiment may have failed to see a sulfur p band that crosses E_F.

ACKNOWLEDGMENTS

This research was supported in part by the National Science Foundation (Grant No. DMR79-25379) and under the National Science Foundation—Materials Research Laboratory program through the Materials Research Center of Northwestern University (Grant No. DMR79-23573), and by the Swiss National Science Foundation. We thank G. A. Benesh and J. von Boehm for helpful discussions.

*Present address: Materials Science Center and Laboratory of Atomic and Solid State Physics, Cornell University, Ithaca, New York 14853.

†Permanent address: Institute of Physics, Beijing, People's Republic of China.

‡Present address: Physics Department, College of William and Mary, Williamsburg, Virginia 23185.

§Present address: EPFL, Laboratoire de Physique Appliquée, CH-1003 Lausanne, Switzerland.

[1] *Physics and Chemistry of Materials with Layered Structure*, edited by F. Levy (Riedel, Dordrecht, 1976), Vols. 2 and 4.

[2] J. A. Wilson and A. D. Yoffe, Adv. Phys. 18, 193 (1969).

[3]E. Tosatti, Festkoerperprobleme 15, 113 (1975).
[4]M. S. Whittingham, Science 192, 1126 (1976).
[5]F. J. DiSalvo and T. M. Rice, Phys. Today 32(4), 32 (1979); Phys. Rev. B 19, 3441 (1979).
[6]F. R. Gamble, F. J. DiSalvo, R. A. Klemm, and T. H. Geballe, Science 168, 568 (1970).
[7]R. B. Murray and A. D. Yoffe, J. Phys. C 5, 3038 (1972).
[8]H. W. Myron and A. J. Freeman, Phys. Rev. B 9, 481 (1974).
[9]P. Krusius, J. von Boehm, and H. Isomäki, J. Phys. C 8, 3788 (1975); J. von Boehm, H. Isomäki, and P. Krusius, Phys. Scr. 22, 523 (1980); J. von Boehm and H. Isomäki, J. Phys. C 13, 3181 (1980); H. Isomäki and J. von Boehm, *ibid.* 14, L75 (1981).
[10]A. Zunger and A. J. Freeman, Phys. Rev. B 16, 906 (1977); D. E. Ellis and A. Seth, Int. J. Quantum Chem. Symp. 7, 223 (1973).
[11]D. W. Bullett, J. Phys. C 11, 4501 (1978).
[12]A. H. Thompson (private communication); R. R. Chianelli, J. C. Scanlon, and A. H. Thompson, Mater. Res. Bull. 10, 1379 (1975).
[13]Details may be found in C. J. Umrigar, Ph.D. thesis, Northwestern University, 1981 (unpublished). The basic film LAPW method is presented in H. Krakauer, M. Posternak, and A. J. Freeman, Phys. Rev. B 19, 1706 (1979); the bulk LAPW method is developed in D. D. Koelling and G. O. Arbman, J. Phys. F 5, 2041 (1975); O. K. Andersen, Phys. Rev. B 12, 3060 (1975).
[14]D. J. Chadi, and M. L. Cohen, Phys. Rev. B 8, 5747 (1973).
[15]G. Lehman and M. Taut, Phys. Status Solidi B 54, 469 (1972).
[16]J. Rath and A. J. Freeman, Phys. Rev. B 11, 2109 (1975).
[17]L. F. Mattheiss, Phys. Rev. B 8, 3719 (1973).
[18]G. A. Benesh (private communication); G. A. Benesh and A. M. Woolley (unpublished).
[19]D. L. Greenaway and R. Nitsche, J. Phys. Chem. Solids 26, 1445 (1965).
[20]D. W. Fischer, Phys. Rev. B 8, 3576 (1973).
[21]P. B. Perry, Phys. Rev. B 13, 5211 (1976); A. R. Beal and W. Y. Liang, Philos. Mag. 27, 1397 (1973); J. Phys. C 6, L482 (1973); W. Y. Liang, G. Lucovsky, R. M. White, W. Stutius, and K. R. Pisharody, Philos. Mag. 33, 492 (1976); A. R. Beal, J. C. Knights, and W. Y. Liang, J. Phys. C 5, 3531 (1972).
[22]A. H. Thompson, K. R. Pisharody, and R. F. Kochler, Jr., Phys. Rev. Lett. 29, 163 (1972).
[23]A. H. Thompson, Mater. Res. Bull. 10, 915 (1975).
[24]R. H. Friend, D. Jérome, W. V. Liang, J. C. Mikkelsen, and A. D. Yoffe, J. Phys. C 10, L705 (1977).
[25]J. A. Wilson, Solid State Commun. 22, 551 (1977).
[26]J. A. Wilson, Phys. Status Solidi 86, 11 (1978).
[27]A perturbative calculation of relativistic corrections, utilizing OPW wave functions, leads to an increase of the *p-d* gap by only 0.02 eV; J. von Boehm (private communication).
[28]The data through 1977 are reviewed by G. V. Subba Rao and M. W. Schafer, in *Intercalated Layered Materials,* edited by F. Levy (Reidel, Dordrecht, 1979), Vol. 6, p. 99.
[29]J. V. McCanny, J. Phys. C 12, 3263 (1979).
[30]O. Jepsen, J. Madsen, and O. K. Andersen, Phys. Rev. B 18, 605 (1978); also see Krakauer *et al.* in Ref. 13.
[31]T. Eguchi, C. Marinos, J. Jonas, B. G. Silbernagel, and A. H. Thompson, Solid State Commun. 38, 919 (1981), and references therein.
[32]P. M. Williams and F. R. Shepherd, J. Phys. C 6, L36 (1973).
[33]G. K. Wertheim, F. J. DiSalvo, and D. N. E. Buchanan, Solid State Commun. 13, 1225 (1973).
[34]C. Webb and P. M. Williams, Phys. Rev. B 11, 2082 (1975).
[35]C. H. Chen, W. Fabian, F. C. Brown, K. C. Woo, B. Davies, B. Delong, and A. H. Thompson, Phys. Rev. B 21, 615 (1980).